



# Photometric and spectroscopic monitoring, radial velocities and evolutionary status of the chromospherically active, close eclipsing binaries ST Centauri and V0775 Centauri

D.J.W. Moriarty<sup>1</sup> · A. Liakos<sup>2</sup> · M.J. Drinkwater<sup>1</sup> · A. Mohit<sup>1</sup> · S.M. Sweet<sup>3,4</sup> · J.F. West<sup>5</sup>

Received: 10 August 2019 / Accepted: 3 December 2019 / Published online: 31 December 2019  
© Springer Nature B.V. 2019

**Abstract** We have combined photometric and spectroscopic observations of two very close eclipsing binary systems, ST Centauri and V775 Centauri, to determine their evolutionary state from calculations of masses and radii and other properties. Spectral types were determined and radial velocities calculated from spectra obtained with the Australian National University's 2.3 m telescope and Wide Field Spectrograph. The spectral type of the ST Cen primary component is F8 IV and the secondary is F8-8.5 IV. The ST Cen mean masses and radii of  $1.40 \pm 0.05 M_{\odot}$  and  $1.38 \pm 0.10 M_{\odot}$  and  $2.2 \pm 0.1 R_{\odot}$  and  $2.13 \pm 0.08 R_{\odot}$  for the primary and secondary components respectively, indicate that they are close to terminal age on the Main Sequence. Although the spectra of V775 Cen appeared to be single lined, the broadening function method enabled us to determine the radial velocities of the faint secondary component as well as those of the primary star. The mean masses and radii of the V775 Cen components are  $1.65 \pm 0.31 M_{\odot}$  and  $0.72 \pm 0.29 M_{\odot}$  and  $1.68 \pm 0.11 R_{\odot}$  and  $1.24 \pm 0.08 R_{\odot}$  for components 1 and 2 respectively. Our data show that V775 Cen is a close Algol binary system, with a secondary

component that has evolved beyond terminal age Main Sequence, has filled its inner critical equipotential surface and is transferring mass to the primary star. The masses and radii of both components of V775 Cen are smaller than those of other Algol binary systems. Although the primary component of V775 Cen is on the Main Sequence, its spectral type is F0/F1 class IV. Both systems displayed episodes of photospheric and chromospheric activity. This was evident in the H $\alpha$  lines of ST Cen and the Na I D lines of the components in both systems. Narrow Na I D lines between those of the binary components suggest that circumbinary gas is present.

**Keywords** Broadening function · Eclipsing binary evolution · Sodium D line emission · H $\alpha$  emission

## 1 Introduction

In their introduction to IAU Symposium 240 on binary stars as critical tools and tests in contemporary astrophysics, Guinan et al. (2007) wrote: "It is crucial to study binary and multiple stars because the vast majority of stars (>50%) in our Galaxy and in other galaxies consist, not of single stars, but of double and multiple star systems. To understand galaxies we need to understand stars, but since most are members of binary and multiple star systems, we need to study and understand binary stars". Mass exchange can be very rapid at some stages within close binaries, so the evolution of such stars differs from that of widely separated binaries and single stars. Many important stellar phenomena are the result of interacting close binaries, e.g. supernovae Type Ia, novae, X-ray binaries and cataclysmic variables. The evolution of close, interacting binaries—generally those with periods less than a few days—is complex and thus there are differing theoretical models (Eggleton 2012; Stępień and Kiraga 2013;

✉ D.J.W. Moriarty  
d.moriarty@uq.edu.au

<sup>1</sup> School of Mathematics and Physics, The University of Queensland, Queensland, 4072, Australia

<sup>2</sup> National Observatory of Athens, Institute for Astronomy, Astrophysics, Space Applications and Remote Sensing, Metaxa and Vas. Pavlou St., 15236, Penteli, Athens, Greece

<sup>3</sup> Centre for Astrophysics and Supercomputing, Swinburne University of Technology, Mail H30, PO Box 218, Hawthorn, VIC 3122, Australia

<sup>4</sup> ARC Centre of Excellence for All Sky Astrophysics in 3 Dimensions (ASTRO 3D), Australia

<sup>5</sup> Astronomical Association of Queensland, P.O. Box 6101, St. Lucia, Queensland, 4067, Australia

Podsiadlowski 2014). In their review of the evolution of close binary systems, Yakut and Eggleton (2005) listed 72 contact binaries, 25 near contact binaries and only 11 detached, close binaries for which reliable data were available for determining their absolute properties.

In this paper we compare the analysis of two close, interacting binaries: ST Centauri, which has a period of 1.22 days and components with very similar luminosity, and V775 Centauri, which has a period of 0.66 days and a secondary component that contributes only about 8% of the luminosity. The rapid, tidally-locked rotations of the ST Cen and V775 Cen component stars would generate magnetic fields causing them to be spotted and to display chromospheric activity, linked to the photospheric spots, as Frasca et al. (2002) found, for example, with RT Lacertae (an RS CVn type of eclipsing binary).

ST Cen is a detached, close binary noted for its variability in brightness outside of eclipse. It was studied by Milone and Hrivnak (1981), who reported the spectral types of both components to be about F9 and developed solutions to light curves, based on photoelectric photometry, which indicated the component stars had radii about twice solar and thus had evolved off the Main Sequence. O'Connell (1951) included ST Cen in his study of eclipsing binary systems where the magnitude at the second quadrature (phase 0.75) was brighter than that at phase 0.25; this is now referred to as the "O'Connell effect". Dryomova et al. (2005) listed ST Cen in a catalogue of RS CVn systems, the principal features of which include asymmetry in light curves, variability in orbital period due to stellar winds linked to strong magnetic fields and chromospheric activity indicated by emission in Balmer and some metal lines, in particular H $\alpha$  and the Ca II K & H doublet. However, Milone and Hrivnak (1981) did not observe signs of emission and commented that the earliness of the ST Cen spectral types was not typical of RS CVn systems, where one component is generally a late G or K spectral type star and luminosity class IV or III. The reasons for the photometric variability in the depths of eclipses and at maximum light between eclipses have not been explained.

V775 Cen has a bright primary component ( $V = 9.74$  mag) catalogued as F0 IV, and a faint secondary component that was not detected in early photometric work, as the period given in earlier editions of the General Catalogue of Variable Stars (GCVS) was 1.327286 days with a deep secondary minimum. A shallow secondary minimum and a period of 0.6636414 days was determined by one us (DM) in 2011–2013 (Streamer et al. 2015). In the current edition of the GCVS, the period is 0.6636425 days, with a shallow secondary minimum depth of 0.14 in the V band (Samus et al. 2017). No information has been available on the spectral type of the secondary component. Like ST Cen, V775 Cen also displayed variability in its light curves. Before we observed the system spectroscopically, our preliminary

modelling using only light curves indicated that V775 Cen was probably a semi-detached binary. With these conditions, chromospheric activity could be expected to occur.

The Na I D doublet is an indicator of chromospheric activity, as neutral sodium lines are much stronger in stars of mid to late K spectral type than other metal lines, and therefore enable comparisons of both stars in binaries with relatively faint late spectral type secondary components with weak Balmer lines. Although emission in the cores of the Ca II H and K and H $\alpha$  lines are the main indicators of magnetic activity in solar and stellar chromospheres, other lines are also important, including the Na I D resonance doublet, e.g. see Gray and Corbally (2009), Houdebine et al. (2009) and Buccino et al. (2014).

The aims of our study were to (1) determine the spectral types of the components of both binary systems; (2) model the light curves of both systems based on multiband photometry and spectroscopic radial velocities and calculate their absolute parameters; (3) to seek evidence for mass transfer and chromospheric and photospheric activity that could explain the variability in light curves; and (4) to determine the evolutionary status of the component stars.

## 2 Observations and methods

### 2.1 Photometry

Photometric observations were made at the Glen Aplin observatory located at 750 m altitude at latitude 28.75° S and longitude 151.85° E. The instruments used for photometry were a 356 mm Celestron Edge HD 1400 aplanatic Schmidt Cassegrain telescope and a Moravian G3-6303 CCD camera with Johnson B and V and Bessel I filters. Reference stars that were photometrically constant and similar in magnitude were chosen in the same field of view as the target variables. The photometric standard star positions and magnitudes are given in Table 1. The Johnson B and V and Sloan  $g$  and  $i$  magnitudes were taken from the AAVSO Photometric All-Sky Survey (APASS) data release 9 (Henden et al. 2015). The near infrared magnitudes were converted to the Cousins ( $I_c$ ) magnitudes from the Sloan  $g$  and  $i$  values with the formula  $I_c = I - 0.3645 - 0.0743 \times (g - i) + 0.0037 \times (g - i)^2$  (Munari et al. 2014). The images were reduced using aperture photometry with MAXIMDL v5 (see Moriarty (2015) for more details of the photometric methods). The standard deviations of magnitudes of the check stars varied from 0.004 and 0.008 mag.

Between 2014 and 2018, 19 times of minimum of ST Cen and eight of V775 Cen were calculated in PERANSO<sup>1</sup> from a 7th order polynomial fit to the light curves spanning about two hours each side of the minima. The follow-

<sup>1</sup><http://www.peranso.com/>.

**Table 1** Magnitudes of the comparison and check stars used to standardise those of ST Cen and V775 Cen. Magnitude uncertainties are shown in brackets below the respective values

Target	Reference star	RA (2000)			Dec (2000)			<i>B</i>	<i>V</i>	<i>I<sub>c</sub></i>
		h	m	s	°	'	"			
ST Cen	HD 299696 <sup>a</sup>	11	10	32.4	−52	34	18.4	10.329 (0.017)	10.255 (0.006)	10.158 (0.058)
ST Cen	HD 97147 <sup>a</sup>	11	10	18.5	−52	19	44.0	10.280 (0.014)	10.206 (0.009)	10.157 (0.079)
V775 Cen	HD 121835 <sup>b</sup>	13	59	18.1	−51	53	34.2	8.89 (0.017)	8.423 (0.013)	7.85
V775 Cen	TYC 8275-1974-1 <sup>a</sup>	13	58	19.8	−51	47	05.5	11.93 (0.060)	10.75 (0.044)	9.66 (0.072)

<sup>a</sup>Source: APASS DR9 (Henden et al. 2015)

<sup>b</sup>Source: Tycho2 spectrally fitted magnitudes (Pickles and Depagne 2010); uncertainties are for the Tycho B and V magnitudes

ing ephemerides, which were used in this paper, were determined from the minima timings: Time of minimum

$$(T_n) = \text{HJD } 2457484.98877 (\pm 0.00024) \\ + 1.2233970 (\pm 0.0000006) (\text{days}) * E_n$$

for ST Cen and

$$T_n = \text{HJD } 2457900.03263 (\pm 0.00045) \\ + 0.6636423 (\pm 0.0000002) \text{ days} * E_n$$

for V775 Cen (Appendix 1 Tables 6 and 7).

In this paper, star 1 of each binary is the primary star, which is eclipsed at phase 0, the primary (i.e. deeper) minimum, and star 2 is the one eclipsed at phase 0.5, the secondary minimum. In the case of ST Cen, the magnitude during the primary eclipse was usually, but not always, fainter than that typically observed at the secondary eclipse; the ST Cen star 1 is the component that was eclipsed at phase 0, epoch HJD 2457484.98839.

## 2.2 Spectroscopy

Spectra were obtained with the stellar aperture of the wide field spectrograph (WiFeS) on the Australian National University (ANU) 2.3 m telescope at Siding Spring Observatory (Dopita et al. 2007; Dopita et al. 2010). Observation dates were: 2016 April 21–23; 2017 February 13 & 14; April 9 & 11; May 15; June 12; July 10; 2018 April 27 & 30; May 2 & 31; June 1–2; July 29–31. Radial velocities were determined from spectra obtained with the B7000 grating, with a velocity resolution of 45 km s<sup>−1</sup> and wavelength range from 4180 to 5300 Å. The B3000 grating was used for spectral typing, as it has a larger wavelength range that includes the Ca II H and K lines. The Ne–Ar arc lamp was used for wavelength calibration; the precision of the wavelength calibration was

improved by observing arc spectra before and after sets of target spectra. Spectra were reduced with PYWIFES, a data reduction pipeline that was written for the WiFeS (Childress et al. 2014).

One dimensional spectra were extracted from the data cubes produced by the PYWIFES routines using a 0 or 1 pixel radius around the spatial pixel where the target was centred and visualised in QFITSVIEW.<sup>2</sup> This procedure was used also to avoid pixels with noise from probable cosmic ray hits that were not fully removed in the reduction routines. Sky background spectra were extracted from spatial pixels away from those with the stellar spectra in each readout frame. Flux units are ergs cm<sup>−2</sup> s<sup>−1</sup> arcsec<sup>−2</sup> Å<sup>−1</sup>. As the orbital periods of these binary systems are short, exposure times were chosen to give a signal to noise ratio of at least 70, and for most target observations about 100–150, which mitigated the effect of line broadening during the observations. Exposure times for ST Cen were mostly 90, 180 or 240 seconds. A similar range of exposure times was used for several observations of V775 Cen; also exposure times of 300 and 360 seconds were used for many observations of V775 Cen with the B7000 grating for radial velocity calculations to enhance the detection of metal lines of the secondary component, as it is relatively faint.

Spectral types were determined manually with XCLASS supplied with MKCLASS<sup>3</sup> and the spectral libraries in that suite (Gray and Corbally 2014). The spectra were classified initially by visual comparisons with standards in the range of 3700–4600 Å. For spectral typing determinations, the wavelengths of the V775 Cen primary component's spectra at phase 0.5 were corrected to heliocentric values by subtracting the systemic radial velocity of 45 km s<sup>−1</sup>; the spectra of ST Cen did not require correction as its systemic veloc-

<sup>2</sup><http://www.mpe.mpg.de/~ott/dpuser/qfitsview.html>.

<sup>3</sup><http://www.appstate.edu/~grayro/mkclass>.

**Table 2** Equivalent widths of pertinent lines in the ST Cen spectra displayed in Figs. 1, 2 and 3

ST Cen Fig. 1; Uncertainty $\pm 0.02$			ST Cen H $\alpha$ ; Uncertainty $\pm 0.01$		
Star, phase	Equivalent widths		Fig. 2, phase	Equivalent widths	
	Fe I $\lambda 4046$	Sr II $\lambda 4077$		Star 1	Star 2
Star 1, 0.50	0.78	1.03	2a, 0.00		1.30
Star 2, 0.00	0.67	0.88	2b, 0.50	1.81	
HD 94964	0.97	0.79	2c, 0.25	0.67	0.61
			2d, 0.24	0.74	0.67
			2e, 0.74	1.04	0.65
			2f, 0.73	1.12	0.66
			2g, 0.25	0.77	0.90

ST Cen Na I D; Uncertainty $\pm 0.01$						
Fig. 3, phase	Equivalent widths					
	Star 2 D <sub>2</sub>	Star 2 D <sub>1</sub>	Star 1 D <sub>2</sub>	Star 1 D <sub>1</sub>	Cb <sup>a</sup> D <sub>2</sub>	Cb <sup>a</sup> D <sub>1</sub>
3a, 0.00	0.71	0.59				
3b, 0.50			0.69	0.60		
3c, 0.25		0.31	0.31		0.18	0.08
3d, 0.24		0.39	0.34		0.09	0.03
3e, 0.74	0.25			0.35	0.10	0.03
3f, 0.73	0.26			0.41	0.10	0.01
3g, 0.25		0.30	0.32		0.18	0.08

<sup>a</sup>The narrow lines due to possible circumbinary gas are abbreviated Cb

ity was close to zero (see Table 4). The spectrum of the ST Cen primary component (star 1) obtained at phase 0.5 (i.e. when it eclipsed star 2), and the spectrum of its secondary component (star 2) at phase 0, were compared with those of standard stars between F8 V and G1 V stars, observed with the same equipment. The eclipses are not complete and thus there was a small proportion of light from the eclipsed star at each phase (e.g. see Fig. 12b). A spectrum of HD 400, an F8 IV star, was also used for comparison.

The spectra of the V775 Cen primary component were compared with library standards of stars between A8 and F3 and luminosities III, IV and V. The spectra of the reference stars were re-binned to the same resolution as the target spectra using the programme SREBIN0 provided with XCLASS, MKCLASS and their utilities (Gray and Corbally 2014). In order to simplify visual comparisons of spectra, they were rectified to deliver a linear continuum baseline using the ‘Autorectify’ function in the XMK25 display routine in XCLASS. The spectral type of the secondary star could not be determined, as the eclipses of V775 Cen were not complete, and the light of the larger, much brighter primary star dominated the spectra at phase 0.

Equivalent widths of the Fe I 4046 and the Sr II 4077 lines were calculated using the equivalent width function and those of the H $\alpha$  and Na I D lines were calculated with

the deblend function on normalised spectra in the IRAF splot task (Tody 1993). Uncertainties were calculated using the m command in splot to determine variability in the continuum on sections of the spectrum that were clear of large absorption lines. The position of the continuum is a major quantifiable factor affecting equivalent width values. However, as the spectral lines were not well separated with the low to medium resolutions of the WiFeS and the broadening effects of rapid orbital and rotational velocities in these close binary systems, the position of the cursor to select the line centres for the Gaussian fits was also an important source of uncertainty where blended lines were not clearly separated.

Radial velocities were calculated with the broadening function (BF) in RAVESPAN (Rucinski 1992 and 2002; Pilecki et al. 2017). The broadening function method was developed to determine radial velocities of short period binary systems in which their rapid rotation rates, synchronised with the orbital velocities, cause substantial broadening of their spectral lines (Rucinski 2004). A synthetic spectrum supplied with the RAVESPAN software was used as the template for the BF (Coelho et al. 2005). Effective temperature settings were varied to suit the expected spectral types;. The wavelength range of 4170–5540 Å was observed with the B7000 grating in the WiFeS. The CONVERT.PY routine in RAVESPAN was modified and used to apply a barycen-



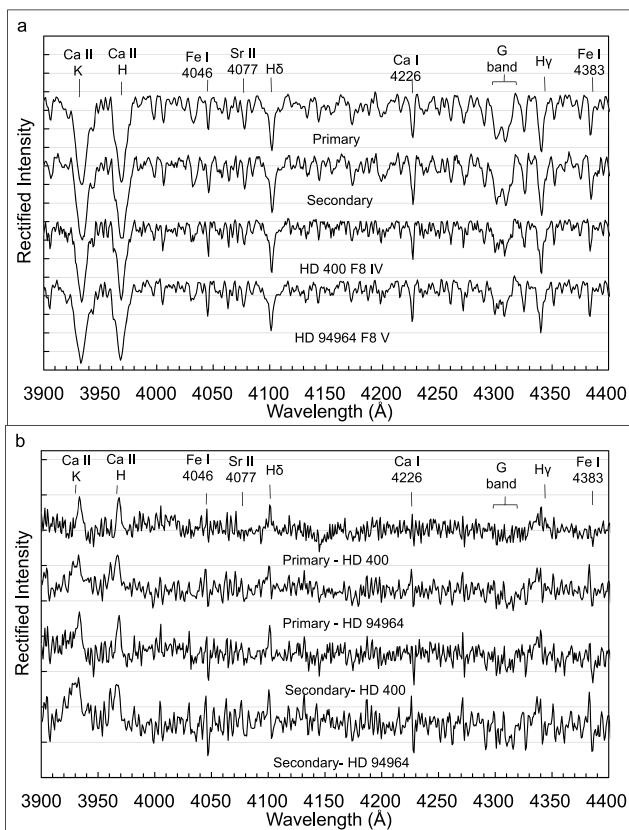


**Fig. 1** Comparison of ST Cen spectra during periods with moderately low chromospheric activity with F8 IV and F8 V stars. **(a)** The primary component (at phase 0.5), 2017 April 11; the secondary component (at phase 0), 2016 April 22. **(b)** Residual values after subtracting the spectra of the standard stars from the ST Cen components' spectra

tric wavelength correction and convert the WiFeS spectra to the format required for RAVESPAN. A 4th order polynomial fit was used with the BF. The spectra were normalised in RAVESPAN to minimise effects of emission lines.<sup>4</sup>

For ST Cen, the template temperature was set at 6000 K and the full wavelength range was used. There was little difference in results if a mask was applied to exclude the broad Balmer lines, thus allowing a wider range of wavelengths to be analysed which lowered the uncertainty values. The gravity coefficient was set at 3.5 and metallicity 0.0.

For V775 Cen, template temperature settings of 7000, 5000, 4500 and 4000 K were tested. Optimum settings to determine the BF values of the secondary component were found to be 4500 K with the gravity coefficient set at 3.0, metallicity at 0.0 and a wavelength range from 4600–5540 Å, with the H $\beta$  line masked. Broadening function values appropriate for the primary component were calculated using a temperature setting of 7000 K, the full wavelength range with the Balmer lines masked, the gravity coefficient 3.5 and metallicity 0.0.

<sup>4</sup><http://www.astro.utoronto.ca/~rucinski/SVDcookbook.html>.

## 3 Analyses and results

### 3.1 Spectroscopic line and spectral type analyses

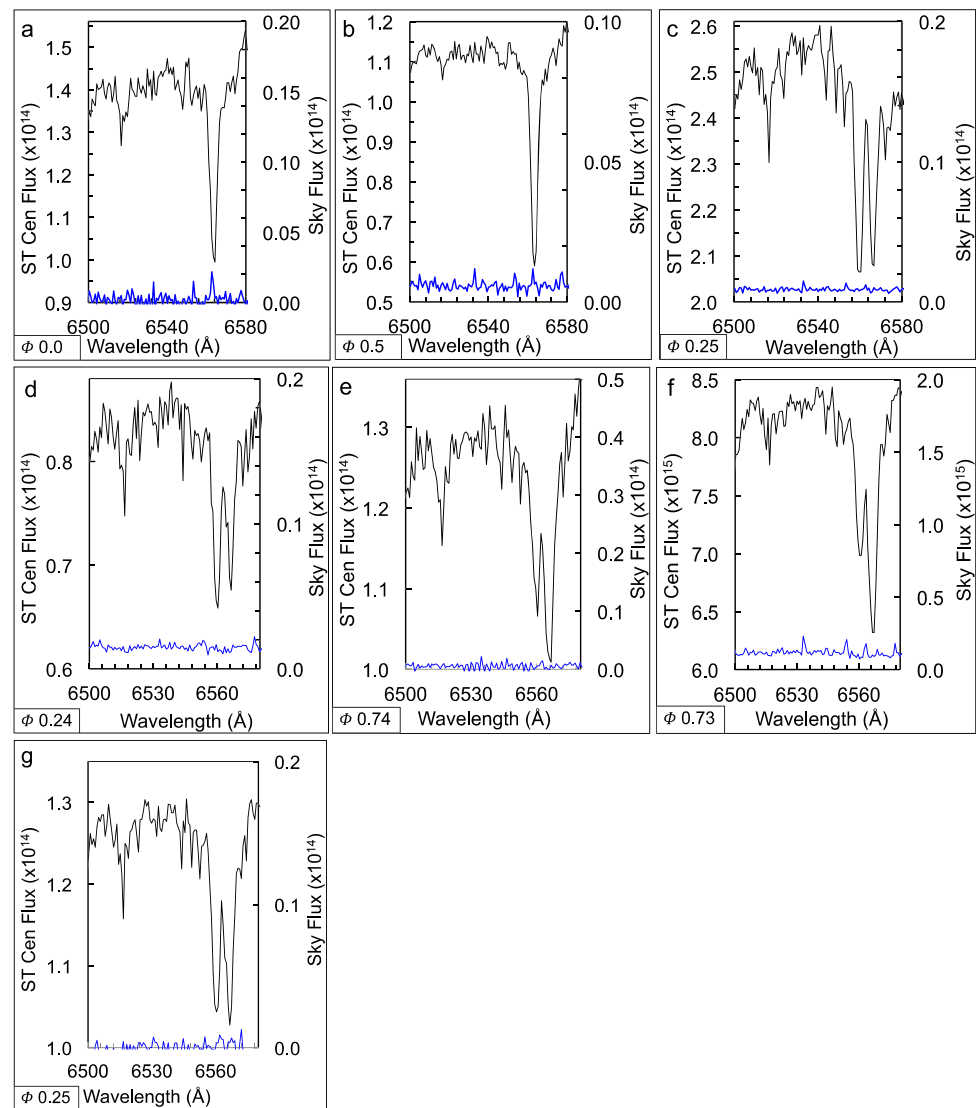
#### 3.1.1 ST Cen

The spectra of both components of ST Cen are similar to those of F8 V and F9 V stars, but differ in that the strength of the Sr II 4077 line is greater than Fe I 4046 line (Fig. 1a). Equivalent widths of the Sr II 4077 lines were greater than those of the Fe I 4046 lines in both components of ST Cen, whereas the Sr II 4077 line was weaker in HD 92976, an F8 V star observed with the same equipment (Table 2). In late F stars, the strength of the Sr II 4077 line relative to the Fe I 4046 line is an important luminosity criterion (Gray and Corbally 2009, p. 226). Spectral typing comparisons of ST Cen components with those of standard stars between F8 V and G1 V and of HD 400, an F8 sub-giant, indicate that the spectral type of star 1 is F8 IV and that of the star 2 about F8–8.5 IV, although the match was not as good for the Ca II H and K lines of star 2 (Fig. 1b).

Chromospheric activity was evident in ST Cen on several occasions, with infilling or variability in the depths of the Na I D doublet, and H $\alpha$  lines (Fig. 2). As both of the ST Cen components are similar in spectral type and luminosity, their H $\alpha$  and Na I D absorption lines should be similar in depth if there were no infilling due to emission resulting from flares or other effects of chromospheric activity. The equivalent width of the H $\alpha$  line of the secondary star (star 2) during the primary eclipse on 2017 June 12 was 30% less than that of the primary star during the secondary eclipse on 2017 July 7 (Table 2). Infilling of the star 2 H $\alpha$  line due to chromospheric activity is also indicated by its weaker depth compared to that of star 1 relative to the nearby metal lines (Fig. 2a and 2b). At phase 0.25 on 2016 April 21, the H $\alpha$  line of star 2 was a little less than that of star 1, which was approaching with a blue shift at that phase (Fig. 2c). On the following night the difference was a little more obvious (Fig. 2d). On some nights, the H $\alpha$  line of the secondary star was markedly infilled, as observed on 2017 February 14 and a year later on 2018 May 31 (see Figs. 2e and 2f and Table 2). Two nights after the latter night, the H $\alpha$  line of the secondary star was stronger than that of the primary component and the equivalent width of that line was larger in star 2 than star 1, which indicates that star 1 was active that night and not star 2 (Fig. 2g and Table 2).

The sodium D doublet lines at the same phases and times as those recorded for the H $\alpha$  lines provide a different view of activity in ST Cen. The relative depths and equivalent widths of the D<sub>1</sub> and D<sub>2</sub> lines were similar during primary and secondary eclipses, however as the eclipses were not total, a

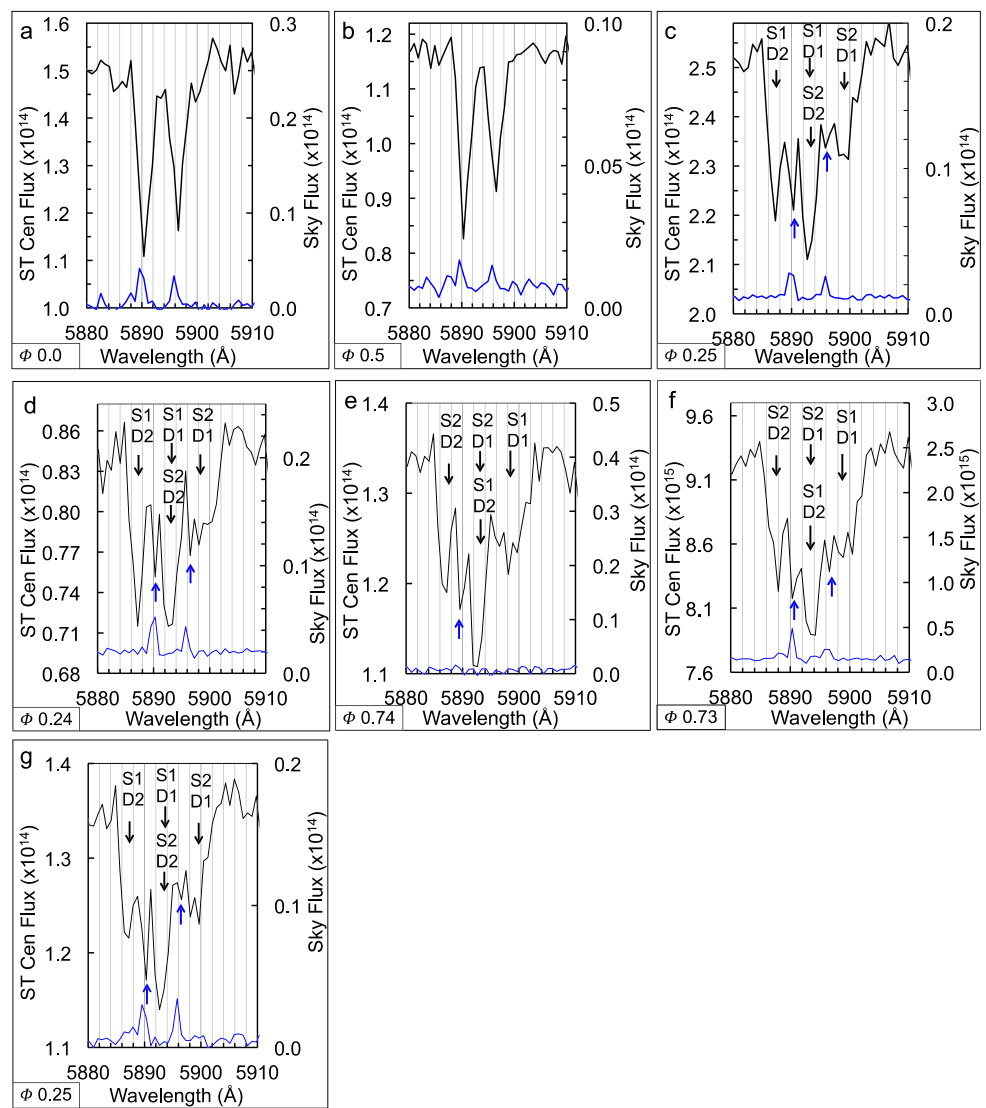
**Fig. 2** Variability in H $\alpha$  absorption lines in ST Cen. The blue line is the sky background flux on each night at the scale on the right axis. Resolution = 7000. Phases ( $\phi$ ) are shown on each panel. Dates and exposure times: (a) 2017 June 12, 90 s. (b) 2017 July 7, 90 s. (c) 2016 April 21, 180 s. (d) 2016 April 22, 90 s. (e) 2017 February 14, 90 s. (f) 2018 May 31, 240 s. (g) 2018 June 2, 240 s



small proportion of light from the eclipsed star was visible at each eclipse (Fig. 3a, 3b and Table 2). The flux intensities were mostly two orders of magnitude larger than the sky background flux. During the first quarter, when the primary component (star 1) is approaching, its Na I D<sub>2</sub> line is partially separated with a blue shift and conversely, the D<sub>1</sub> line of star 2 is separated with a red shift from the blend of their complementary lines in the central position (Figs. 3c, 3d and 3g). At the second quarter, with star 1 receding, the line positions are reversed (Figs. 3e and 3f). The equivalent width values that we determined with the deblend function in splot provide an approximate indication of the relative depths of the sodium lines (Table 2). The uncertainty values in Table 2 apply to the noise in the continuum. The low equivalent widths of 0.25 and 0.26 for the star 2 D<sub>2</sub> lines support the evidence of the H $\alpha$  line equivalent widths that the secondary component was very active on 2017 February 14 and 2018 May 31, as shown in Figs. 2e and 2f.

The Na I D lines are not only indicators of chromospheric activity, but also of the presence of circumbinary gas. Narrow absorption lines at or close to the systemic velocity of ST Cen (see Table 4) at  $\lambda$ 5890 and  $\lambda$ 5896, are apparent in these spectra. The fact that the absorption depths are 1–2 orders of magnitude greater than the background noise and sky emission lines suggest that they are associated with the binary system and are not due to interstellar absorption. Further support for this conclusion is given by the presence of similar lines in the Na I D spectra of V775 Cen with slightly longer wavelengths consistent with its larger systemic velocity (Sect. 3.1.2). The D<sub>2</sub> circumbinary line was moderately well separated on several nights from the binary component lines with an equivalent width that ranged from about 15% to 50% of the star 1 and star 2 D<sub>2</sub> values (Table 2). The D<sub>1</sub> was blended more closely with the star lines and thus the equivalent width values are only approximate.

**Fig. 3** Variability in Na I D doublet absorption lines in ST Cen and sky background flux at the corresponding phases and times to the H $\alpha$  spectra in Fig. 2. (S1 = star 1; S2 = star 2; D1 = Na I D<sub>1</sub>; D2 = Na I D<sub>2</sub>). Black arrows mark the calculated D line positions at each phase. Blue upward arrows mark absorption lines indicating probable circumbinary gas. Resolution = 7000. Phases ( $\phi$ ) are shown on each panel. Dates and exposure times as in Fig. 2



### 3.1.2 V775 Cen

The spectrum of the primary component of V775 Cen, is similar to that of the F0 IV standard star HD 142908 and less so to HD 8829, an F0 V star (Fig. 4). At spectral type F0, the primary luminosity criteria are the blends of the ionised iron and titanium, including the Fe II and Ti II  $\lambda$ 4172-9 (Gray and Corbally 2009). The blend of lines  $\lambda$ 4172-9 is similar in the spectra of V775 Cen and HD 142908, whereas it is weaker in the F0 V star HD 8829 (Fig. 4). The Sr II  $\lambda$ 4077 line, although less sensitive to luminosity at F0 than at F8, was stronger in V775 Cen than in HD 8829 (Fig. 4). The closest match of the V775 Cen spectra to those of stars between A8 and F3 and luminosities III, IV and V in the MK-CLASS libraries was with F0 IV.

As the luminosity of the primary star is much greater than that of star 2, any emission in absorption lines in the blue band due to the secondary star could be difficult

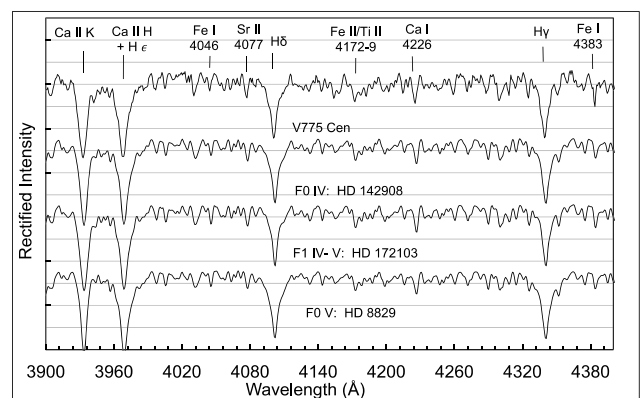
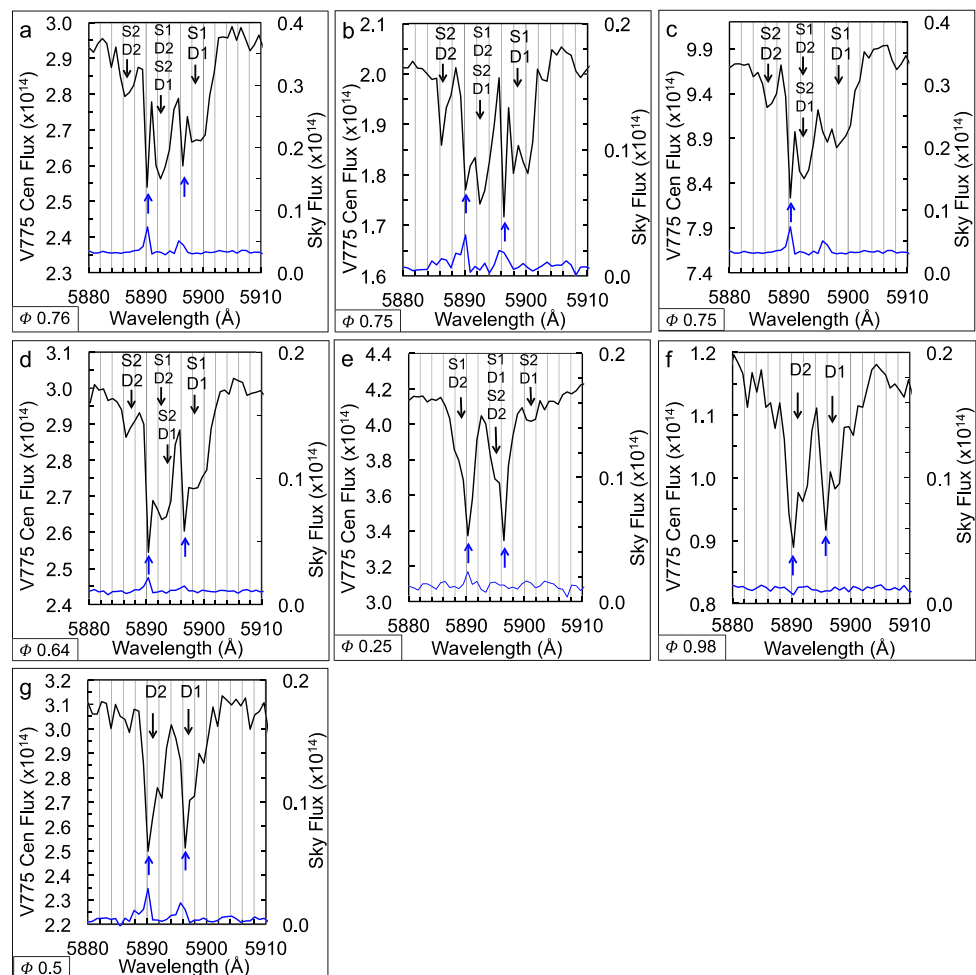


**Fig. 4** V775 Cen spectra. Comparisons of spectra at phase 0.5 on 2016 April 21 with F0 IV, F1 IV-V and F0 V standard stars;  $R = 3000$

to distinguish from noise at the 7000 resolution we used. Therefore, we analysed the Na I D spectra to seek indica-

**Fig. 5** Variability in the Na I D doublet of V775 Cen; the sky background flux is shown with a blue line. The spectrum of HD 92976, an F0 IV star, was observed with the same equipment. (a) 2017 May 16; 100 s. (b) 2017 June 12; 90 s. (c) 2016 April 22, 350 s. (d) 2018 May 31; 350 s. (e) 2017 July 7; 120 s. (f) 2017 April 11; 100 s. (g) 2017 June 12; 90 s. Abbreviations, labels and resolution as in Figs. 2 and 3



tions of chromospheric activity. The combination of the  $45 \text{ km s}^{-1}$  systemic velocity and the orbital velocities of  $90$  and  $215 \text{ km s}^{-1}$  of stars 1 and 2 respectively (Sect. 3.2) permitted separation of the Na I D lines to some extent, depending on phase and exposure times, as shown in Fig. 5. The depths of the Na I D lines and infilling in the cores varied between nights. In particular, the equivalent widths of the D<sub>1</sub> line of star 1 varied from  $0.37 \pm 0.01$  to  $0.49 \pm 0.01$  and those of the D<sub>2</sub> line of star 2 varied from  $0.09 \pm 0.09$  to  $0.14 \pm 0.01$  around the second quadrature phase (Table 3).

During the primary eclipses, the centres of the D<sub>1</sub> and D<sub>2</sub> lines were partially infilled at the systemic velocity, with a narrow absorption line on the blue side (Fig. 5f). A similar, although less obvious, pattern was observed during all primary eclipses (not shown here) and also at phase 0.5 when the secondary star was almost fully eclipsed (Fig. 5g). The fact that this infilling was centred at the systemic velocity during the eclipses indicates that it occurred in the central cores of the Na D lines and thus was most likely due to chromospheric activity.

Narrow absorption lines similar to those observed in the ST Cen spectra, but close to  $\lambda 5890.5$  and  $\lambda 5896.6$ , were ap-

parent, particularly in the spectra with the shorter exposure times of 90–120 s (Fig. 5a and Fig. 5b). Their equivalent widths varied about twofold (Table 3). These narrow lines were blended with the lines of the primary star at phase 0.25 (Fig. 5e). The shift in wavelength by about  $45 \text{ km s}^{-1}$  to the red from the rest wavelengths indicates that these lines were due to gas travelling at the systemic velocity of V775 Cen (Sect. 3.2). Variations in velocity of the narrow lines around the systemic velocity would be expected for circumbinary gas rather than for interstellar gas. As shown for example by Popper (1988) the interstellar absorption lines are very weak. Absorption lines of circumbinary sodium would be more intense in disks around eclipsing binary systems than in systems with low inclination angles. A study of both ST Cen and V775 Cen at much higher spectral resolution is needed to confirm the presence of circumbinary gas.

### 3.2 Radial velocity calculations

The velocities of the two components of ST Cen at the quadrature phases are well separated by the broadening function, with no indication of a third star being present, i.e.



**Table 3** Equivalent widths of pertinent Na I D lines of V775 Cen spectra in Fig. 5 and during eclipses on two other nights. Uncertainty  $\pm 0.01$ 

Figure, date	Phase	Equivalent widths						
		Star1 D <sub>1</sub>	Star 2 D <sub>2</sub>	Star 2 D <sub>1</sub>	Cb <sup>a</sup> D <sub>1</sub>	Cb <sup>a</sup> D <sub>2</sub>	D <sub>1</sub>	D <sub>2</sub>
5a, 2017 May 16	0.76	0.41	0.09		0.06	0.05		
5b, 2017 June 12	0.75	0.49	0.14		0.14	0.08		
5c, 2016 April 22	0.75	0.44	0.13		0.11	0.06		
5d, 2018 May 31	0.64	0.37	0.09		0.10	0.09		
5e, 2017 July 07	0.25			0.09				
5f, 2017 April 11	0.98						0.73	0.65
5g, 2017 June 12	0.50						0.58	0.56

<sup>a</sup>The narrow lines due to possible circumbinary gas are abbreviated Cb

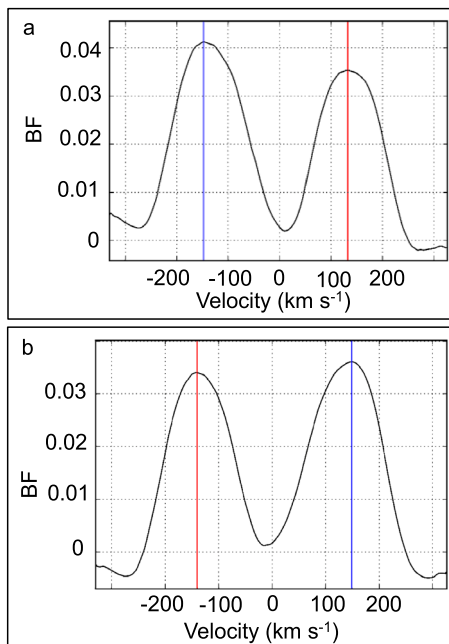


**Fig. 6** Broadening function (BF) analyses of ST Cen. The peak velocity of the more massive component is marked with the blue line and that of the other with the red line. (a) Phase 0.25. (b) Phase 0.75

a velocity peak near  $0 \text{ km s}^{-1}$  (Fig. 6a and 6b). The lower values for the broadening function of the secondary component indicate its luminosity is a little less than that of the primary star.

Radial velocities of the V775 Cen secondary component at the quadrature phases were not distinguishable from noise with template settings appropriate for the primary star (Figs. 7a and 7b). The velocity of the faint component of V775 Cen was marginally apparent with an effective temperature of 7000 K when the Balmer lines were masked (Figs. 7c and 7d). However, the velocity signal of the secondary star was clearly evident when an effective temperature of 4500 K and a lower gravity setting, which would be likely for an evolved K4 or K5 star, were used together with

wavelengths longer than  $4600 \text{ \AA}$  (Figs. 7e and 7f). The BF values of the V775 Cen primary component were lower with the Balmer lines masked and with  $T_{\text{eff}} = 4500 \text{ K}$ . However, BF values for secondary component could not be determined for many of the observed spectra without masking out the H $\beta$  line and all lines at wavelengths shorter than  $4600 \text{ \AA}$ .

The radial velocity curves modelled in PHOEBE (see Sect. 3.3.2) and the data points plotted against the phases of each system calculated photometrically are shown in Fig. 8. The uncertainty bars show the RMS scatter of the data points calculated with RAVESPAN. Although radial velocities were determined at a range of phases in addition to the quadratures, several spectra were not used in the analyses as they were very noisy, as shown for example in Figs. 2, 3 and 5, due to a greater intensity of photospheric and chromospheric activity on those nights.

### 3.3 Photometric analyses

#### 3.3.1 Intrinsic variability

ST Centauri displayed intense photospheric activity on several occasions, with variability in magnitudes in each photometric pass band at maximum light between eclipses and also in the depths of primary and secondary minima. For example in 2018, ST Cen at phase 0.75 was 20–30 mmag brighter in May than in March (Fig. 9). Standard deviations in the brightness of the check star in each band varied between 4 and 10 mmag, which indicates that the variability in ST Cen was intrinsic to that system and not due to seeing conditions. The  $B-V$  and  $B-I$  colour indices at phase 0.75 were 0.60 and 1.36 respectively in 2018 March 15 and 0.64 and 1.40 in 2018 May 19 respectively. The primary eclipse in each wavelength band observed in 2017 was deeper than those observed in 2016 and 2018 (see Fig. 10).

V775 Centauri also displayed photospheric activity with variability particularly noticeable in the blue pass band. Some examples of the variability were evident on the nights chosen for the light curve modelling (see Fig. 11).

**Fig. 7** Broadening function (BF) analyses of V775 Cen. Phases, template temperature and gravity settings are shown. (a) and (b): wavelength range 4170–5540 Å. (c) and (d): wavelength range 4600–4840 Å. (e) and (f): wavelength range 4880–5540 Å

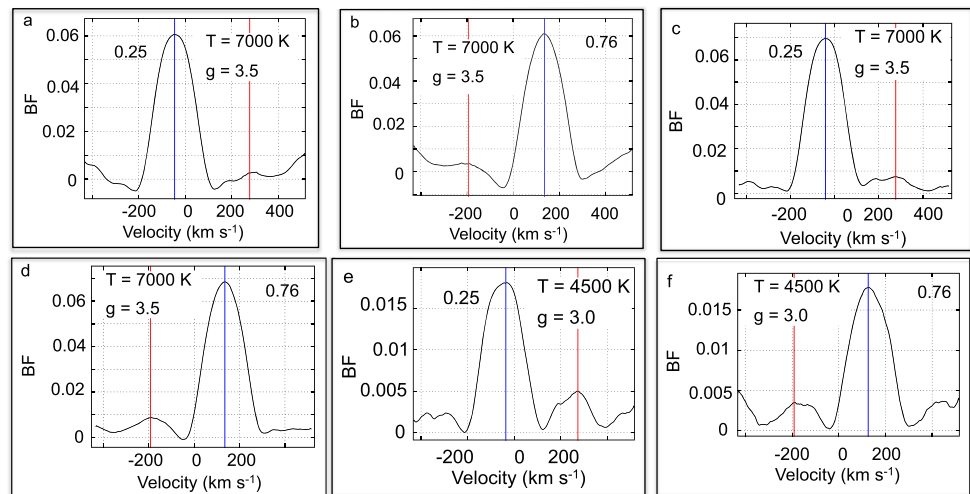
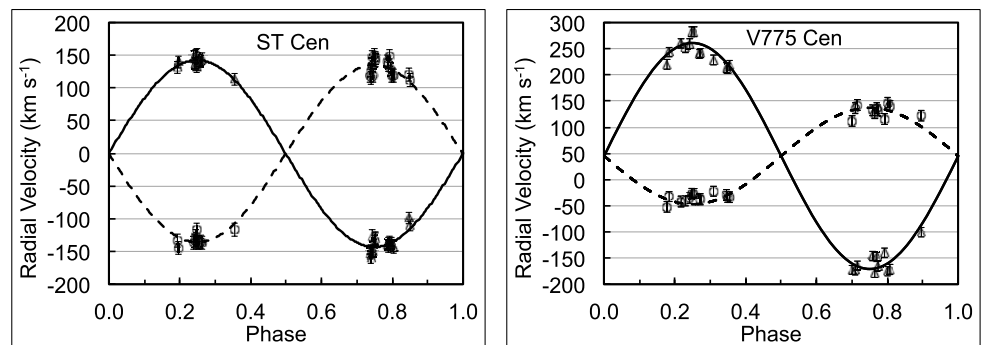


**Fig. 8** Radial velocities ST Cen (left) and V775 Cen (right). Dashed and solid lines denote the fit of the data points for the primary and secondary components respectively



### 3.3.2 Analyses of light and radial velocity curves

The light curves and radial velocity curves of the binary systems were analysed with PHOEBE v.0.29d software (Prša and Zwitter 2005), which uses the 2003 version of the Wilson–Devinney code (Wilson and Devinney 1971; Wilson 1979, 1990). The results of the modelling are shown in Table 4. The temperature of the ST Cen primary component was set at 6200 K, a value between the effective temperatures of F8 spectral classes (Gray and Corbally 2009). The temperature of the V775 Cen star 1 was set at 7250 K, appropriate for an F0 star. The temperature of the secondary star in both systems was adjusted during the modelling processes. The values of bolometric albedos ( $A$ ) and gravity darkening coefficients ( $g$ ) were set as  $A = 0.5$  and  $g = 0.32$  for convective atmospheres and  $A = 1$  and  $g = 1$  for radiative atmospheres appropriate to the temperature of each component (Lucy 1967; Rucinski 1969). Synchronous rotation was assumed, so the synchronization parameters  $F1$  and  $F2$  were set as 1. The linear limb-darkening coefficients,  $x$ , were taken from the tables of van Hamme (1993); the dimensionless potentials  $\Omega_1$  and  $\Omega_2$ , the fractional luminosity of the primary component  $L1$  and the inclination  $i$  of the systems' orbits were set as adjustable. The mass

ratio ( $q(m_2/m_1)$ ) of each system was calculated from the orbital velocities of their component stars. Other abbreviations used in Table 4 are as follows; system parameters: epoch of primary minimum  $T_0$ , orbital period  $P_{orb}$ , systemic velocity  $V_0$ ; component parameters:  $a$  semi major axis,  $K$  radial velocity amplitude,  $r$  fractional radii.

Spots were added to obtain good fits of the models to asymmetry in the light curves, and given that the systems exhibit magnetic activity hot spots were selected as being more appropriate than cool spots. As brightness often varied at the maxima in both systems, hot spots were set on the secondary star surfaces in the ST Cen models and on the primary star's surface in the V775 Cen models; the spot parameters (co-latitude, co-longitude, radius, and temperature factor) were adjusted. Cool spots on the opposite binary could be added as an alternative to fitting the light curves, but they would not be in agreement with the spectra we observed.

The absolute parameters of the components were calculated using the ABSPAREB software (Liakos 2015). Three-dimensional representations of the binary systems were prepared in BINARY MAKER 3.0.<sup>5</sup>

The available photometric data for ST Cen were split into four sets because the variability in flux, especially around

<sup>5</sup><http://binarymaker.com/>.

**Table 4** Light curve and radial velocity parameters for both binary systems. Uncertainties in brackets apply to the last digit. <sup>a</sup> fixed, <sup>b</sup> assumed

		ST Cen			V775 Cen	
System parameters						
Mode	Detached			Semi Detached		
$i$ (°)	85.2 (1)			76.5 (3)		
$T_0$ (HJD)	2457484.98877 <sup>a</sup>			2457900.032625 <sup>a</sup>		
$P_{\text{orb}}$ (d)	1.223397 <sup>a</sup>			0.6636423 <sup>a</sup>		
$q$ ( $m_2/m_1$ )	0.98 (0.02)			0.42 (0.06)		
$V_0$ (km s <sup>-1</sup> )	1 (2)			45 (2)		
Component parameters						
	Primary	Secondary	Primary	Secondary	Primary	Secondary
$a$ (R <sub>☉</sub> )	3.29 (0.06)	3.46 (0.05)	1.2 (0.2)	2.9 (0.2)	1.2 (0.2)	2.9 (0.2)
$K$ (km s <sup>-1</sup> )	138 ± 2	141 ± 2	90 ± 12	216 ± 16	90 ± 12	216 ± 16
$T_{\text{eff}}$ (K)	6200 ± 150 <sup>a</sup>	6100 ± 200	7250 ± 150 <sup>a</sup>	4450 ± 115	7250 ± 150 <sup>a</sup>	4450 ± 115
$\Omega$	4.14 (8)	4.12 (5)	3.05 (3)	2.71 (1)	3.05 (3)	2.71 (1)
$A_{a,b}$	0.5	0.5	1	0.5	1	0.5
$g_{a,b}$	0.32	0.32	1	0.32	1	0.32
$r$ (pole)	0.312 (7)	0.311 (5)	0.377 (5)	0.286 (2)	0.377 (5)	0.286 (2)
$r$ (point)	0.35 (1)	0.35 (1)	0.42 (1)	0.412 (2)	0.42 (1)	0.412 (2)
$r$ (side)	0.32 (7)	0.322 (7)	0.393 (6)	0.298 (2)	0.393 (6)	0.298 (2)
$r$ (back)	0.337 (9)	0.338 (8)	0.407 (8)	0.331 (2)	0.407 (8)	0.331 (2)
Parameter						
	<i>B star 1</i>	<i>V star 1</i>	<i>I star 1</i>	<i>B star 2</i>	<i>V star 2</i>	<i>I star 2</i>
ST Cen $x$	0.687	0.553	0.392	0.696	0.561	0.402
ST Cen $L$	0.553 (2)	0.523 (2)	0.492 (2)	0.499 (1)	0.498 (1)	0.512 (1)
V775 Cen $x$	0.584	0.484	0.360	0.962	0.810	0.570
V775 Cen $L$	96 (3)	0.94 (8)	0.85 (6)	0.04 (1)	0.06 (1)	0.15 (1)
Spot parameters of ST Cen						
Date	Star	Co-Latitude (°)	Longitude (°)	Radius (°)	Temperature factor	
2016	2	89	160	17	1.05	
2017	2	89	299	12.0	1.13	
2018 March	2	71	146	15	1.18	
2018 May	2	83	285	21	1.1	
Spot parameters of V775 Cen						
Date	Star	Co-Latitude (°)	Longitude (°)	Radius (°)	Temperature factor	
2015	1	54	186	9	1.14	
2016	1	87	171	12	1.15	
2016	2	93	266	31	0.63	
2017	1	90	228	8	1.08	

the quadrature phases, did not allow a single model to be developed from the combined data sets (Fig. 10). The first set consisted of the light curves observed during a four month

period in 2016, while those obtained within a four week period commencing on 2017 April 29 comprised the second set, which did not show any significant variations between

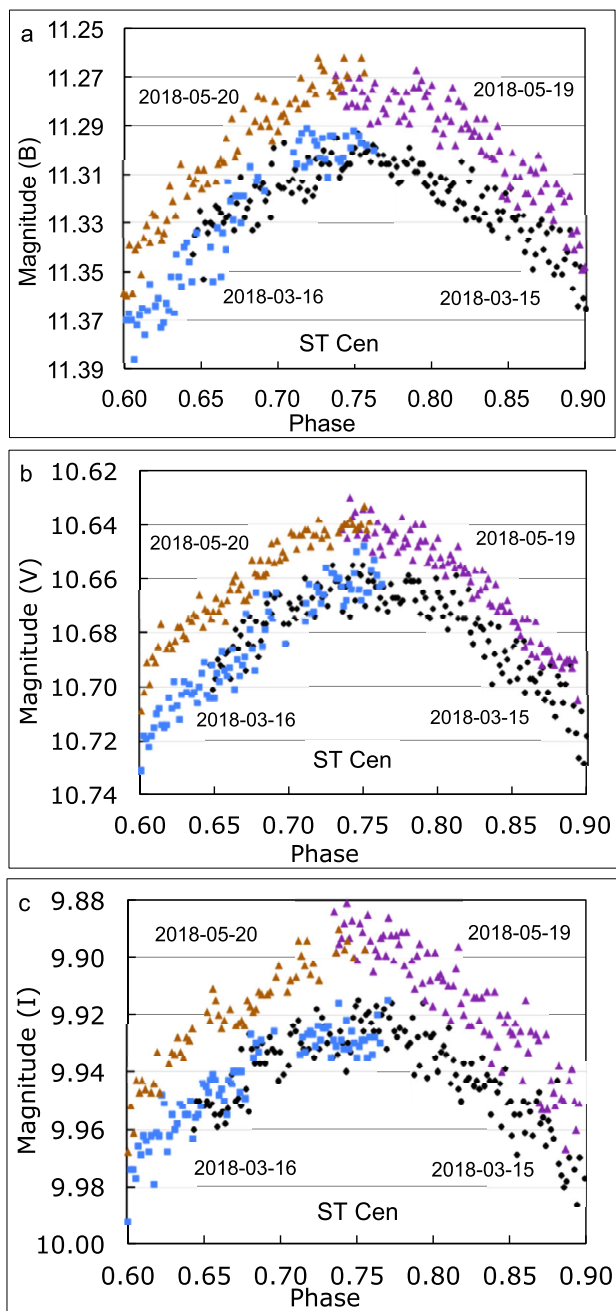


**Fig. 9** Light curve variability of ST Cen in *B*, *V* and *I* pass bands. (a) *B* band, 2018-03-15 (squares, blue), 2018-03-15 (circles, black), 2018-05-20 (triangles, brown), 2018-05-19 (triangles, purple). (b) *V* band; details as in (a). (c) *I* band, details as in (a)

the different phase sections. However, the 2018 light curves in March and May both covered a secondary minimum and maximum, but as there was a significant difference in the secondary maxima between these data sets, they were modelled separately. In particular, the first set of 2018 (March) covers approximately 70% of the total period and its data were obtained over four consecutive nights. The second set in 2018 (May) included 80% of the whole light curve and its

data were obtained during five successive nights. However, the 2018 May set lacked a primary minimum, so its model was based mostly on the model for the 2018 March set with adjustments made to the spot parameters.

The average values for all parameters for the ST Cen photometric models, except those for the spots, were consistent across the three wavelength bands and the four data sets between 2016 and 2018 (Table 4). A hot spot was required on the secondary star in a different position for each set to obtain good fits to the light curves (Table 4).

The modelled light curves of V775 Cen are shown in Fig. 11. The large uncertainties in the values of the model parameters are the result of variability in the spectra due to chromospheric activity in both components and to the low flux of the secondary component and line broadening caused by its rapid rotational and orbital velocities. Consecutive nights of photometric observations were modelled in each year in order to minimise variability in linking observations from different orbital cycles. The models with the best fits to the light curves required a hot spot on the primary component that was in a different position each year (Table 4). The model of the 2016 May 5 light curve also required a large cool spot on star 2 (see Fig. 12f). The effective temperature of 4450 K indicates that star 2 has a spectral type of about K5.

The absolute parameters for ST Cen indicate that both components are evolved and have similar masses and radii with the primary star being slightly larger and brighter (Table 5). The mass of the V775 Cen secondary component is one third that of the primary, but its radius is similar, indicating it is much more evolved than the primary star (Table 5).

As shown in Fig. 12a, both components of ST Cen are close to filling their inner critical equipotential (Roche) surfaces. Similarly, the V775 Cen primary component also has about 90% of that volume filled, whereas in contrast its secondary component has filled its inner critical equipotential surface (Fig. 12d). Some examples showing the positions on the binary images of the spots on the ST Cen and the V775 Cen components are displayed in Fig. 12.

## 4 Evolutionary status

The locations of the ST Cen and V775 Cen components within the Hertzsprung–Russell (HR) and mass-radius evolutionary diagrams are shown in Figs. 13 and 14. The zero and terminal age Main Sequence (ZAMS and TAMS) and the 1.4  $M_{\odot}$  isochrone lines (for solar metallicity composition) for these diagrams were taken from Girardi et al. (2000).

The astrophysical model of ST Cen indicates that both components occupy a position on the HR diagram close to

**Fig. 10** Observed light curves of ST Cen (points, black) and modelled solutions (lines, magenta). (a) 2016; (b) 2017; (c) 2018 March; (d) 2018 May

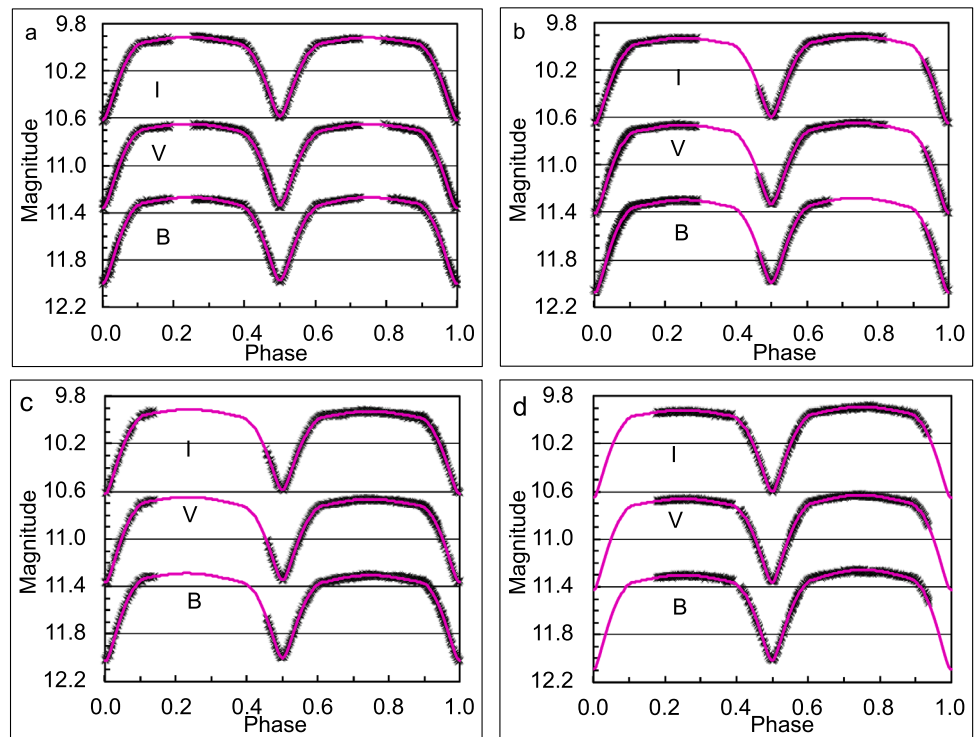
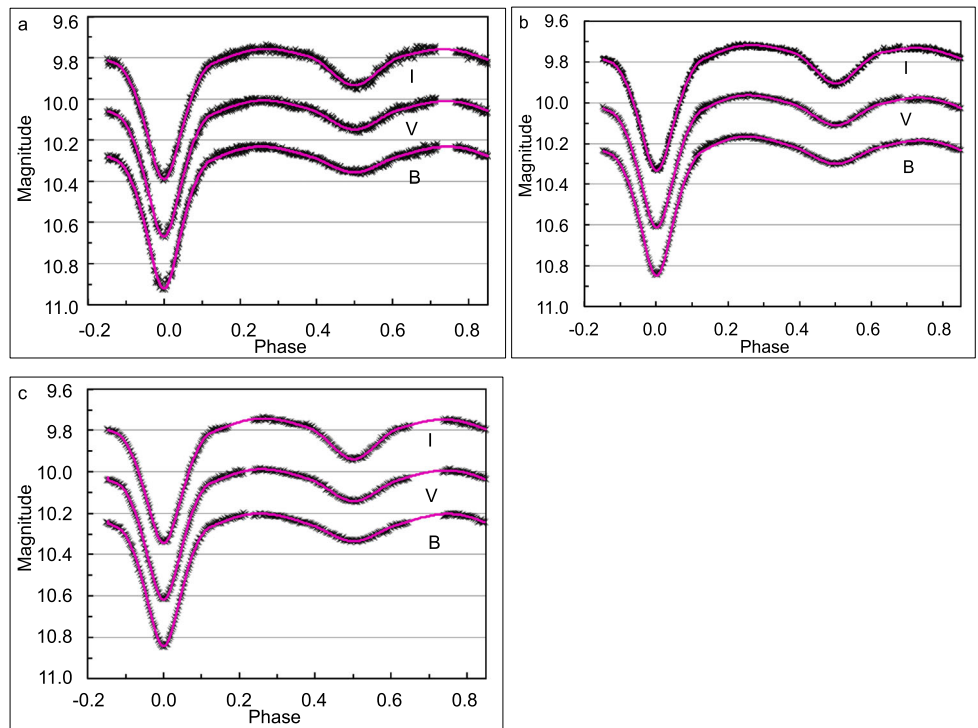


**Fig. 11** Observed light curves of V775 Cen (points, black) and modelled solutions (lines, magenta). (a) 2015; (b) 2016; (c) 2017. The light curves for the V and I bands are offset by +0.25 and +0.5 magnitudes respectively



terminal age MS (Fig. 13). The positions of the ST Cen components on the mass-radius diagram (Fig. 14) differ from those of the detached, close binaries in Fig. 3a of Yakut and Eggleton (2005) and are more similar to those of near contact binaries, although with larger radii. The presence of

flares and chromospheric activity indicate it is likely that both ST Cen stars have strong stellar winds, which would explain the probable presence of circumstellar or circumbinary gas in the ST Cen system, as shown in Fig. 3. Spectra at much higher resolution than we had available would be



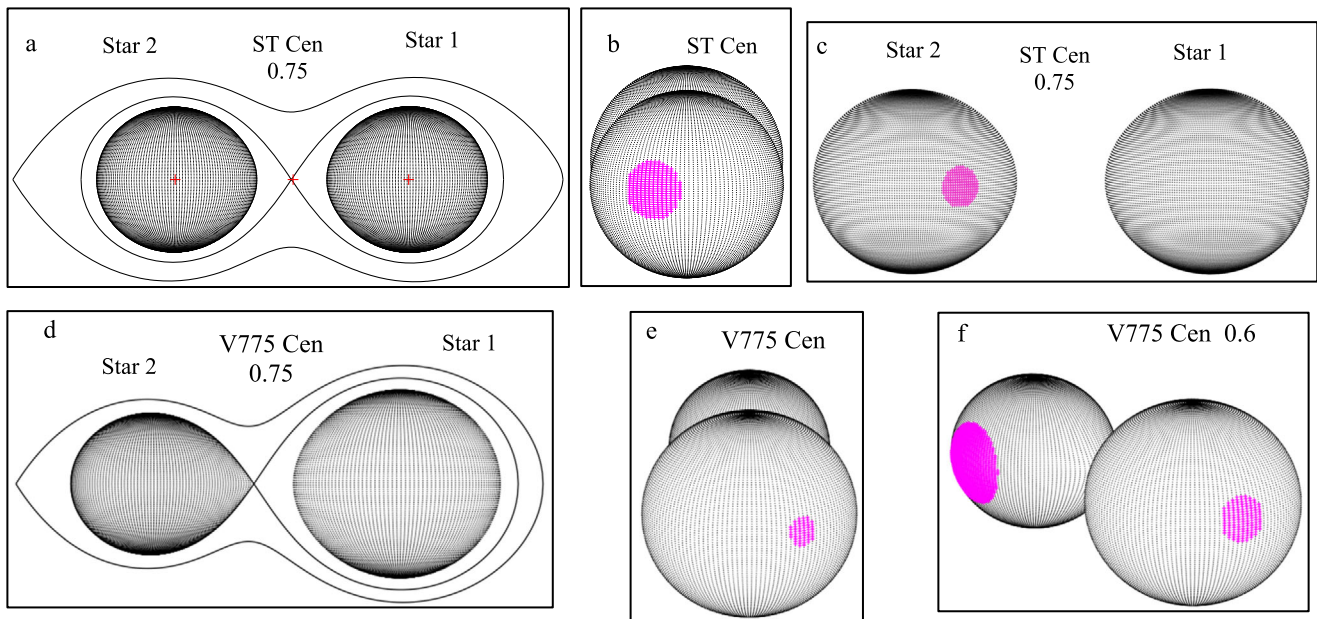


**Fig. 12** Three-dimensional representations of the binary systems. (a) ST Cen inner and outer critical equipotential surfaces; (b) ST Cen 2016, phase 0. (c) ST Cen 2017 May, showing position of the hot spot. (d) V775 Cen inner and outer critical equipotential. (e) V775

Cen, phase 0.5 showing the hot spot on star 1 in 2017. (f) phase 0.6 showing the position of the hot spot on star 1, V775 Cen and the cool spot on star 2 in the 2016 models

**Table 5** Absolute parameters of the ST Cen and V775 Cen component stars. Uncertainties are in brackets

Parameter	ST Cen star 1	ST Cen star 2	V775 Cen star 1	V775 Cen star 2
$M (M_{\odot})$	1.40 (0.05)	1.38 (0.1)	1.65 (0.31)	0.72 (0.29)
$R (R_{\odot})$	2.2 (0.1)	2.13 (0.08)	1.68 (0.11)	1.24 (0.08)
$L (L_{\odot})$	6.4 (0.8)	5.7 (0.7)	6.95 (1.1)	0.54 (0.10)
$\text{Log } g (\text{cm s}^{-2})$	3.90 (0.04)	3.92 (0.05)	4.21 (0.10)	4.11 (0.18)
$M_{bol} (\text{mag})$	2.7 (0.8)	2.9 (0.9)	2.6 (0.9)	5.4 (1.0)

required for a more detailed analysis of circumbinary gas in both ST Cen and V775 Cen.

The positions of the V775 Cen components on the mass-radius diagram are similar to those of near contact binaries plotted in Fig. 3a of Yakut and Eggleton (2005). Our modelling results show that the V775 Cen primary star is close to filling its inner critical equipotential surface and thus is more evolved than indicated by its position on the Main Sequence (Fig. 13). The secondary star has left the Main Sequence, is much more evolved than the primary, and has filled its inner critical equipotential (Roche) surface and, therefore, is transferring mass to the current primary star. V775 Cen is, therefore, in the category of the SD2 near contact, or typical Algol, binaries discussed by Yakut and Eggleton (2005) and Stepień and Kiraga (2013), where the originally more massive primary star fills its inner Roche surface and transfers mass to the original secondary star with a consequent reversal of the mass ratio. The presence of hot spots on the primary component and the episodes of emission displayed in the sodium D lines confirm that mass transfer is continuing.

The narrow sodium D lines indicate that circumbinary gas is probably present orbiting and impacting on the primary star, as would be expected for a typical Algol-type binary system.

## 5 Discussion and conclusions

In their review of the evolutionary processes of close binary stars, Yakut and Eggleton (2005) discussed double-lined spectroscopic binary systems, as it is only for those systems that accurate mass ratios can be determined. As mentioned in Sect. 1, their sample sizes were small, especially for detached close binaries and near contact binaries. It is also important to have not only radial velocities, but also high quality photometric light curve data to minimise uncertainties due to non-Keplerian effects when determining absolute parameters of the systems.

One of the problems in obtaining data to determine the absolute masses and radii of binary components is being able to determine the radial velocities of faint secondary

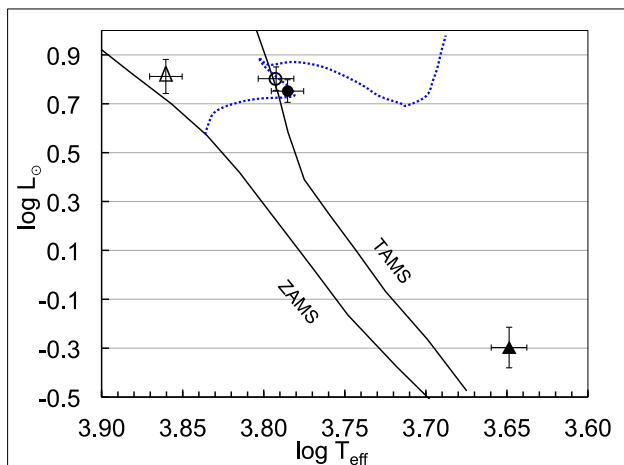


**Fig. 13** The position of the components of ST Cen (star 1 = open and star 2 = filled circles) and V775 Cen (star 1 = open and star 2 = filled triangles) relative to the zero and terminal age Main Sequence tracks (ZAMS and TAMS) on the Hertzsprung–Russell diagram. The evolutionary track of a single  $1.4 M_{\odot}$  star is shown for comparison (dotted blue line)

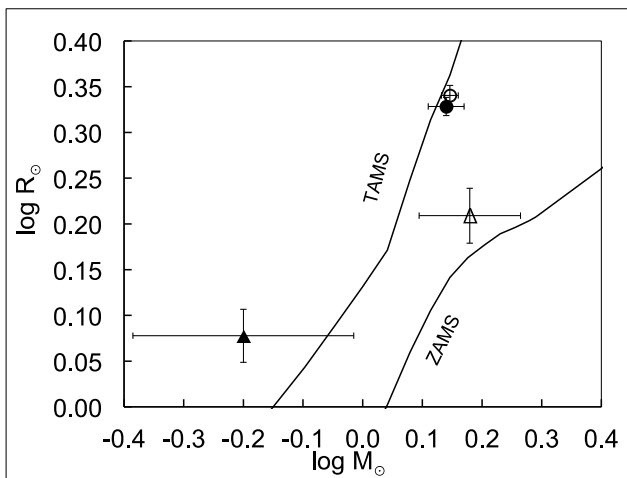


**Fig. 14** Positions of the components of ST Cen and V775 Cen on the Mass-Radius diagram. Symbols are as in Fig. 13

components in binaries that are referred to as single lined. The spectral lines of a low mass secondary star, which in a close binary would be rotating very rapidly, are broadened and obscured by those of the bright primary star. In the case of V775 Cen, velocities of the secondary component could not be distinguished using the cross correlation function and its two dimensional variant, TODCOR (Zucker and Mazeh 1994). However, as we have shown in this paper, the broadening function developed by Rucinski (2002) can be used to determine radial velocities of both components of apparently single lined binaries where the flux of the secondary star is a low proportion of the system flux.

Both of the components of ST Cen and V775 Cen have convective outer regions and their rotation rates, locked to

their orbital velocities, are very rapid compared to single stars of the same spectral types and therefore would exhibit intense magnetic dynamo activity (see Berdyugina 2005). Such activity causing cool and hot spots would explain the short term photometric variability observed in both ST Cen and V775 Cen (Figs. 9, 10 and 11). Further study of these systems at much higher spectral resolution would be rewarding. Variable episodes of infilling due to emission in the  $H\alpha$  lines (Fig. 2) mean that caution is needed when using ratios of the Balmer lines to metal lines to discern the spectral types of the ST Cen system. We chose data from nights with apparently lower signs of chromospheric activity for spectral typing.

Asymmetry and variability in the ST Cen light curves, as shown for example by the light curves in the B, V and I bands in Fig. 9, are indeed prominent features, which were discussed by Milone and Hrivnak (1981). Similar variability was also observed around the 0.25 phase quadrature (data not shown). The period of ST Cen that we determined is only slightly different from 1.2233930 days given in the current edition of the General Catalogue of Variable Stars (Samus et al. 2017). The small variations in epochs of minimum are within the range associated with the effect of star spots. Kalimeris et al. (2002) showed that star spots caused high frequency, low amplitude variability in the O–C diagram, generally less than 0.01 days. The best fits with the modelling were obtained when bright (hot) spots were included on star 2. Frasca et al. (2002) studied  $H\alpha$  emission in RT Lac, and attributed it at phase 0.75 to the presence of bright chromospheric plages associated with spots in the photosphere facing the observer at that phase. As shown in Fig. 12c, a good fit to our models of the ST Cen 2017 May data included a hot spot on the hemisphere facing the observer at the phase 0.75. The position of the hot spots was different on other occasions. It is probable that the emission was due to similar events in the chromosphere of both component stars on some nights, e.g. on 2016 April 22 as shown by infilling of the  $H\alpha$  lines (Fig. 2 and Table 2). Although good fits to the light curves were obtained by fitting a hot spot to the secondary component during the modelling, it is probable that both components are spotted as evidenced by the photometric variability. For each year, hot spots in the equatorial zone on the facing hemispheres of each component could also be fitted, with minor adjustments to the other spot positions or temperature factors. These are consistent with the short term variability in the light curves (Fig. 9) and spectral data showing chromospheric activity, especially at the quadrature phases when the facing zones were visible to the observer (Figs. 2 and 3).

In summary, our modelling results for ST Cen confirm the conclusion of Milone and Hrivnak (1981) that both components are close to terminal age on the Main Sequence. Although ST Cen is a chromospherically active system with

episodes of emission in the Na I D and Balmer lines, and its photospheres are active with variations of 10–30 millimagnitudes, it is not a typical RS CVn system. We did not find evidence for strong emission in the Ca II H and K lines and both components have similar masses, radii and spectral types. The similar broadening function values for both components also show that their luminosities are similar (Rucinski 2002). Typical RS CVn binary systems display strong emission in the H and K lines and their secondary components have evolved into the Hertzsprung gap, with much larger radii than their primary components (Popper and Ulrich 1977).

Our results show that V775 Cen is a semi-detached Algol binary with the secondary component filling its inner critical equipotential surface and transferring mass to the primary F0 IV component. Variability and infilling in its Na I D lines indicate that both components are chromospherically active; they also display photospherical activity. In considering the modelling of the evolution of cool close binaries by Stepień (2011), we estimate that the probable initial masses of the current primary and secondary components of V775 Cen could have been about  $0.7 M_{\odot}$  and  $1.3 M_{\odot}$  respectively. There would have been a period of rapid, large scale mass transfer when star 2 first filled its inner critical Roche surface and mass ratio reversal occurred. There is no indication

of a period change since 1980 as shown by the low values for the observed-calculated times of minima; the uncertainties of the ASAS data are unknown, but would be large, as the times of minima were fitted from observations at various intervals over a full season, not single nights (Appendix 1 Table 7). Unfortunately, there are not enough minima timings prior to 1980 that would allow an orbital period analysis and calculation of the mass transfer rate for this system.

**Acknowledgements** We thank Dr. Bogumil Pilecki for his assistance in installing RAVESPAN and Dr. Pierre Maxted for editing the conversion script to suit the WiFeS instrument, including barycentric velocity corrections. We are grateful to Troy Cobb, Yannik Rist, Lize Coetzee and Christine Moriarty for their assistance with observations on the ANU 2.3 m telescope. We thank the handling editor and referee for their many helpful comments, which have improved the paper. This research made use of the VizieR catalogue access tool and the SIMBAD database, operated at CDS, Strasbourg, France, and the AAVSO Photometric All-Sky Survey (APASS), funded by the Robert Martin Ayers Sciences Fund. We acknowledge grants from the Edward Corbould Research Fund of the Astronomical Association of Queensland to DJWM for assistance with the purchase of equipment and software for photometry and for travel expenses and time on the ANU 2.3 m telescope.

**Publisher's Note** Springer Nature remains neutral with regard to jurisdictional claims in published maps and institutional affiliations.

## Appendix 1

**Table 6** Times of minima of ST Cen. Values for minima are the means of minima in the blue, visible and infrared pass bands. The observed minus calculated (O–C) differences in epochs of minima were determined using a period (P) of 1.223397 days and epoch ( $T_0$ )

2457484.98877 HJD. The linear ephemeris formula is  $T_n = T_0 + E_n P$ , where  $T_0$  is the initial time of minimum, P is the period in days,  $E_n$  is the number of epoch cycles since  $T_0$  and  $T_n$  is the time of minimum after  $n$  cycles

Year*	Cycle	Epoch (HJD)	Uncertainty	O–C	Uncertainty
1977 <sup>a</sup>	–11598	2443173.690		0.000	
2005 <sup>b</sup>	–3274	2453479.589	0.005	0.002	0.005
2013	–857.5	2455435.926	0.001	0.000	0.001
2014	–631	2455713.025	0.001	0.000	0.001
2014	–555	2455806.003	0.003	0.000	0.003
2015	–42.5	2457432.994	0.002	–0.001	0.002
2015	–35	2457442.171	0.007	0.001	0.007
2015	0	2457484.988	0.002	–0.001	0.002
2017	337.5	2457897.886	0.002	0.000	0.002
2017	340	2457900.945	0.001	0.001	0.001
2018	578	2458192.112	0.002	–0.001	0.002
2018	633.5	2458260.010	0.021	–0.001	0.021

\*Notes. Source: (a) Recalculated from Milone and Hrivnak (1981); (b) GCVS (Samus et al. 2017)

**Table 7** Times of primary minima for V775 Cen. The observed minus calculated (O–C) differences in epochs of minima were determined using a period of 0.6636423 days and epoch 2457900.03262. The procedure described by Moriarty (2016) was used to determine several epochs of minimum between 2002 and 2008 from data collected during the All Sky Automated Survey (ASAS) (Pojmański 2002)

Year*	Cycle	Epoch (HJD)	Uncertainty	O–C	Uncertainty
1980 <sup>a</sup>	–20239	2444468.5712		–0.005	
2003 <sup>b</sup>	–7745	2452760.129		0.006	
2004 <sup>b</sup>	–7257	2453077.347		0.003	
2005 <sup>b</sup>	–6479	2453600.303		0.009	
2007 <sup>b</sup>	–5719	2454104.658		–0.004	
2007 <sup>b</sup>	–5185	2454459.044		–0.003	
2010 <sup>c</sup>	–3926	2455294.573	0.003	0.000	0.003
2011	–3166	2455798.941	0.002	0.000	0.002
2011	–3151	2455808.896	0.002	0.000	0.002
2012	–2750	2456075.017	0.001	0.001	0.002
2013	–2170	2456459.928	0.001	–0.001	0.001
2014	–1617	2456826.922	0.001	–0.001	0.001
2015	–1121	2457156.089	0.001	0.000	0.001
2015	–580	2457515.121	0.001	0.001	0.001
2017	0	2457900.033	0.001	0.000	0.001

\*Notes. Source: (a) Wolf and Kern (1983). (b) ASAS. (c) Brát et al. (2011)

## References

- Berdyugina, S.V.: *Living Rev. Sol. Phys.* **2**, 8 (2005)
- Brát, L., et al.: *Open Eur. J. Var. Stars* **137**, 1 (2011)
- Buccino, A.P., et al.: *Astrophys. J. Lett.* **781**, 1 (2014)
- Childress, M.J., et al.: *Astrophys. Space Sci.* **349**, 517 (2014)
- Coelho, P., et al.: *Astron. Astrophys.* **443**, 375 (2005)
- Dopita, M., et al.: *Astrophys. Space Sci.* **310**, 255 (2007)
- Dopita, M., et al.: *Astrophys. Space Sci.* **327**, 245 (2010)
- Dryomova, G., et al.: *Astron. Astrophys.* **437**, 375 (2005)
- Eggleton, P.P.: *J. Astron. Space Sci.* **29**, 145 (2012)
- Frasca, A., et al.: *Astron. Astrophys.* **388**, 298 (2002)
- Girardi, L., et al.: *Astron. Astrophys. Suppl.* **141**, 371 (2000)
- Gray, R.O., Corbally, C.J.: *Stellar Spectral Classification*. Princeton Univ. Press, Princeton (2009)
- Gray, R.O., Corbally, C.J.: *Astron. J.* **147**, 80 (2014)
- Guinan, E.F., Harmanec, P., Hartkopf, W.: *IAU Symp.* **240**, 5 (2007)
- Henden, A.A., et al.: *AAVSO Photometric All-Sky Survey, DR 9* (2015). <http://www.aavso.org/apass>
- Houdebine, E.R., et al.: *Astron. Astrophys.* **503**, 929 (2009)
- Kalimeris, A., et al.: *Astron. Astrophys.* **387**, 959 (2002)
- Liakos, A.: *ASPC* **496**, 286 (2015)
- Lucy, L.B.: *Z. Astrophys.* **65**, 89 (1967)
- Milone, E.F., Hrivnak, B.J.: *Astron. J.* **86**, 1546 (1981)
- Moriarty, D.J.W.: *J. Am. Assoc. Var. Star Obs.* **43**, 151 (2015)
- Moriarty, D.J.W.: *J. Am. Assoc. Var. Star Obs.* **44**, 10 (2016)
- Munari, U., et al.: *J. Astron. Data* **20**, 4 (2014)
- O’Connell, D.J.K.: *Publ. Riverview College Obs.* **2**, 85 (1951)
- Pickles, A., Depagne, E.: *Publ. Astron. Soc. Pac.* **122**, 1437 (2010)
- Pilecki, B., et al.: *Astrophys. J.* **842**, 110 (2017)
- Podsiadlowski, P.: In: González Martínez-País, I., Shahbaz, T., Casares Velázquez, J. (eds.) *Accretion Processes in Astrophysics* (Canary Islands Winter School of Astrophysics), p. 45 Cambridge University Press, Cambridge (2014). <https://doi.org/10.1017/CBO9781139343268.003>
- Pojmański, G.: *Acta Astron.* **52**, 397 (2002)
- Popper, D.M.: *Astron. J.* **95**, 1242 (1988)
- Popper, D.M., Ulrich, R.K.: *Astron. J.* **212**, L131 (1977)
- Prša, A., Zwitter, T.: *Astrophys. J.* **628**, 426 (2005)
- Rucinski, S.M.: *Acta Astron.* **19**, 245 (1969)
- Rucinski, S.M.: *Astron. J.* **104**, 1968 (1992)
- Rucinski, S.M.: *Astron. J.* **124**, 1746 (2002)
- Rucinski, S.M.: *IAU Symp.* **215**, 17 (2004)
- Samus, N.N., et al.: *General Catalogue of Variable Stars: Version GCVS 5.1*. *Astron. Rep.* **61**, 80 (2017)
- Stępień, K.: *Acta Astron.* **61**, 139 (2011)
- Stępień, K., Kiraga, M.: *Acta Astron.* **63**, 239 (2013)
- Streamer, M., et al.: *J. Am. Assoc. Var. Star Obs.* **43**, 67 (2015)
- Tody, D.: In: *Astronomical Data Analysis Software and Systems II*, vol. 52, p. 173 (1993). <http://adsabs.harvard.edu/abs/1993ASPC..52..173T>
- Yakut, K., Eggleton, P.P.: *Astron. J.* **629**, 1055 (2005)
- van Hamme, W.: *Astron. J.* **106**, 2096 (1993)
- Wilson, R.E.: *Astrophys. J.* **234**, 1054 (1979)
- Wilson, R.E.: *Astrophys. J.* **356**, 613 (1990)
- Wilson, R.E., Devinney, E.J.: *Astrophys. J.* **166**, 605 (1971)
- Wolf, G.W., Kern, J.T.: *Astrophys. J. Suppl. Ser.* **52**, 429 (1983)
- Zucker, S., Mazeh, T.: *Astrophys. J.* **420**, 806 (1994)